



Effect of hot rolling and cooling process on microstructure and properties of 2205/Q235 clad plate

Meng Yan¹ · Jing-na Sun¹ · Hua-gui Huang¹ · Lei Chen¹ · Ke Dong² · Zhen-ye Chen³

Received: 12 March 2018 / Revised: 7 October 2018 / Accepted: 9 October 2018 / Published online: 24 October 2018
© China Iron and Steel Research Institute Group 2018

Abstract

The 2205/Q235 clad plate was fabricated by vacuum hot rolling with symmetrical assembling pattern of Q235/2205/2205/Q235. The flow stress behavior and processing map of 2205 duplex stainless steel (DSS) were investigated by hot compressive tests on a Gleeble-3800 simulator. Then, thermal–mechanical coupled nonlinear finite element models of vacuum hot rolling and subsequent cooling process were established. From the simulation results, the influence of rolling reduction and rolling speed on hot deformation state of 2205 DSS in the assembled slab was disclosed and the optimal rolling parameters were presented. Meanwhile, the cooling rate of 2205 DSS under different cooling conditions and thicknesses of the clad plate was obtained. According to the numerical simulation results, pilot experiments were successfully carried out on a laboratory scale. The material universal testing machine, optical microscope, scanning electron microscope and energy-dispersive spectrometer were used to evaluate the mechanical properties and microstructure of bonding interface and 2205 DSS matrix for different rolling reduction and cooling processes. The results showed that with symmetrical assembling pattern, the approximate thermodynamic conditions can be established for 2205 DSS to avoid cracks in hot rolling process. When the rolling reduction increased from 10 to 40%, the shear strength of the bonding interface is increased from 120 to 530 MPa, and the uniform two-phase microstructure of 2205 DSS and satisfactory mechanical properties can be obtained with cooling rate higher than 10 °C/s between 1050 and 500 °C after rolling.

Keywords 2205/Q235 clad plate · 2205 duplex stainless steel · Vacuum hot rolling · Finite element method · Bonding interface · Dual-phase scale

1 Introduction

Duplex stainless steel (DSS) has both the advantage of ferritic stainless steel with high strength and anti-stress corrosion resistance of chloride and the advantage of austenitic stainless steel with excellent toughness and weldability. Thus, it has been widely used in petroleum, chemical, marine equipment, paper making, nuclear power

and other industries [1–3]. However, DSS is expensive, and its hot and cold forming performances are inferior compared with carbon steel [4]. 2205/Q235 duplex stainless steel clad plate has not only the advantage of excellent wear resistance, corrosion resistance, oxidation resistance and long service life of DSS, but also the advantage of high strength–toughness, good mechanical properties and impact resistance of plain-carbon steel. As a more economical material with lower usage of DSS [3], the DSS clad plates have attracted increasing attention in recent years [5–8].

Due to the obviously different plasticity of the dual phases in DSS and the narrow processing temperature window [9, 10], crack occurs easily in the actual production process [11]. Although many efforts, such as explosive welding [12, 13], have been focused on the manufacture of the DSS clad plate, it is still a challenge to obtain satisfactory quality and efficiency. On the other hand, the final

✉ Hua-gui Huang
hhg@ysu.edu.cn

¹ National Engineering Research Center for Equipment and Technology of Cold Strip Rolling, Yanshan University, Qinhuangdao 066004, Hebei, China

² China National Heavy Machinery Research Institute Co., Ltd., Xi'an 710032, Shaanxi, China

³ HBIS GROUP Central Iron and Steel Research Institute, Shijiazhuang 050023, Hebei, China

corrosion resistance of 2205 DSS highly depends on heat treatment process [14]. It requires a rapid cooling rate to avoid phase transformation in the sensitive zone. Fortunately, the present researches indicate that the pack rolling method can provide an approximate isothermal deformation condition for difficult-to-deformation materials, and it has been successfully used in the deformation control of refractory high-temperature alloy, such as titanium alloy, GH720Li, aluminum/magnesium alloy clad plate and other materials [15–18]. Thus, the four-layer symmetrical clad sheet rolling of Q235/2205/2205/Q235 can also customize thermodynamic condition suitable for hot deformation of 2205 DSS, which makes it possible to prepare the DSS clad plate by vacuum hot rolling.

As for the heat treatment after hot roll bonding, the ultra-fast cooling (UFC)-accelerated cooling equipment (ACC) has been successfully developed and applied in medium plate production line [19]. The advanced UFC-ACC system can also provide powerful cooling ability for clad plate. However, the base plate in the clad plate is usually thicker, which hinders the cooling rate improvement of the 2205 clad material in the symmetrically assembled slab of Q235/2205/2205/Q235. In order to achieve the desired cooling route and cooling rate, finite element method can be used to investigate the matching relation between the cooling mode and thickness of Q235 plate. Therefore, the numerical simulation and experiments were carried out to explore the influence of the hot rolling and cooling process on microstructure and properties of 2205/Q235 clad plate by vacuum hot rolling.

2 Experimental and numerical simulation procedure

2.1 Establishment of processing map of 2205 DSS

Based on the Gleeble-3800 thermal–mechanical simulator, the stress–strain curves of 2205 DSS were measured according to the common hot rolling process. The deformation temperature T was from 950 to 1250 °C, and the strain rate $\dot{\epsilon}$ was from 0.01 to 10 s⁻¹. Cylindrical specimens of 8 mm in diameter and 15 mm in height were prepared for hot compression tests. By using the acquired data, the processing map based on dynamic material modeling and specific plastic work approaches would be established.

The chemical compositions of the base material Q235 and the clad material 2205 used in this paper are shown in Table 1.

2.2 Finite element analysis of vacuum hot rolling process

As mentioned above, in order to establish the stable and desired thermodynamic conditions for 2205 DSS in vacuum hot rolling process, as shown in Fig. 1, the Q235/2205/2205/Q235 four-layer symmetrical assembling method was adopted. A nonlinear thermal–mechanical coupled finite element model was set up to disclose the thermodynamics state of 2205 DSS during the vacuum hot rolling process, including the detailed information such as the temperature, strain (ϵ), stress and strain rate. Combining with the processing map of 2205 DSS, the rolling parameters can be evaluated and optimized by judging whether the deformation state is among the range of the allowable hot working process window.

For the convenience of experimental verification, the roller diameter and width were set to be $\phi 200$ mm \times 220 mm which was the same dimension of the experimental roller used in this paper. The slab sizes of 2205 and Q235 were 200 mm \times 100 mm \times 2.5 mm and 200 mm \times 100 mm \times 12.5 mm, respectively. The parameters of finite element model are shown in Table 2. For reducing the complexity and increasing the calculation speed, the stripping agent and sealing were simplified. The roller and slab were set as rigid and plastic body, respectively. The contact frictional coefficient between 2205 and Q235 was 0.30, and that between the steel roller and Q235 plates was 0.25.

2.3 Numerical simulation of cooling process after rolling

In order to investigate the cooling route and cooling rate of 2205 clad material in Q235/2205/2205/Q235 slab, the numerical simulation was carried out on platform of MSC.MARC. As shown in Fig. 2, considering the symmetry, a one-half model for cooling process was established. The initial temperature T_b of clad plate was 1050 °C, and the ending temperature T_e of 2205 DSS in the heat treatment process was 400, 500, 600 and 700 °C, respectively. The thickness of 2205 plate h_2 was 2.0 mm, and the total thickness of clad plate $h_1 + h_2$ was 20, 23, 25, 27 and 30 mm, respectively. According to the laminar cooling technology, the convective heat transfer coefficient between the surface of Q235 plate and water λ_1 was set to be 1.0, 1.5 and 2.8 kW/(m² K), respectively [20], and the bottom surface of 2205 was simplified as symmetrical insulated boundary in this paper. Other material parameters were calculated by JMatPro software.

Table 1 Main chemical compositions of 2205 and Q235 steels (mass%)

Material	C	Si	Mn	Cr	Ni	Mo	N	S	P	Fe
2205	0.02	0.61	1.10	23.04	5.12	3.12	0.18	0.003	0.014	Balance
Q235	0.16	0.26	0.69	0.3	0.27	0.04	0.003	0.035	0.030	Balance

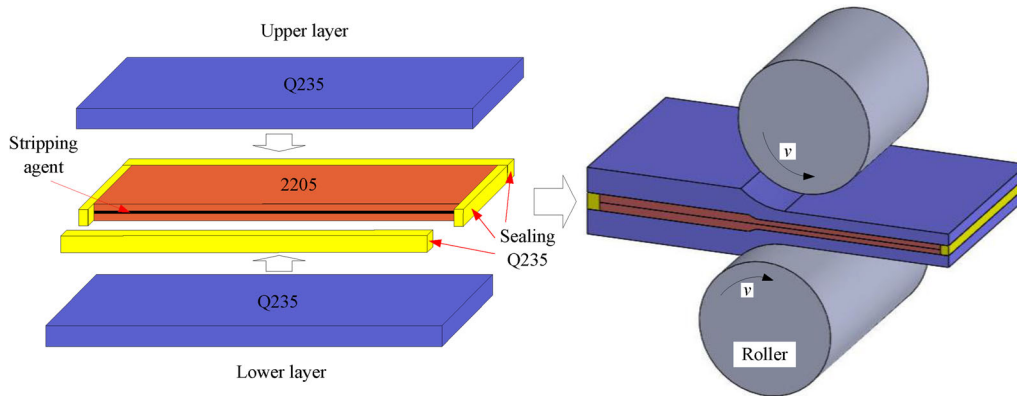


Fig. 1 Schematic diagram of four-layer symmetrically assembled slab for vacuum hot rolling

Table 2 Parameters of finite element model

Parameters	Value
Rolling temperature $T_0/^\circ\text{C}$	1200
Rolling reduction $\Delta h/\%$	10 20 30 40
Rolling speed $v/(\text{m s}^{-1})$	0.01 0.045 0.10 1.00

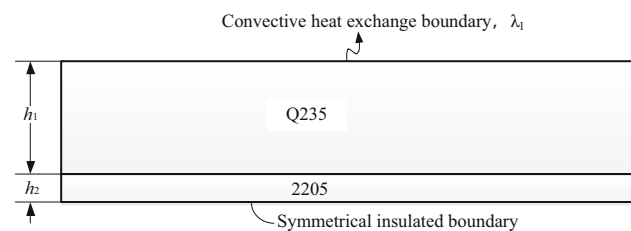


Fig. 2 Finite element model of heat transfer in cooling process of Q235/2205/2205/Q235 slab

2.4 Pilot experiment

In order to verify the proposed rolling parameters, pilot experiments were conducted on a roller with a diameter of 200 mm in National Engineering Research Center for Equipment and Technology of Cold Strip Rolling, Yanshan University. Consistent with the simulation parameters, the sizes of 2205 and Q235 plates were 200 mm × 100 mm × 2.5 mm and 200 mm × 100 mm × 12.5 mm, respectively. After the surface grinding and decontamination, the four-layer symmetrical packing method was used to build the initial rolling slab. The vacuum was pumped to 0.1 Pa by a pressure machine [21].

Figure 3 shows the schematic diagram of hot rolling and heat treatment process which was designed based on the dynamic continuous cooling transformation curves of 2205 DSS [22]. The packed assembled slab was heated and rolled with the optimal rolling parameters and then was cooled down and held at 1050 °C for 30 min. Finally, it was quickly cooled down to 400, 500, 600 and 700 °C, respectively, in 1 min with a rapid cooling mode conducted by a temperature-controlling system. Finally, it was cooled slowly down in air.

2.5 Shear strength and microstructure characterization of bonding interface

As shown in Fig. 4, the shear strength of bonding interface was tested according to Chinese standard GB/T 6396-2008

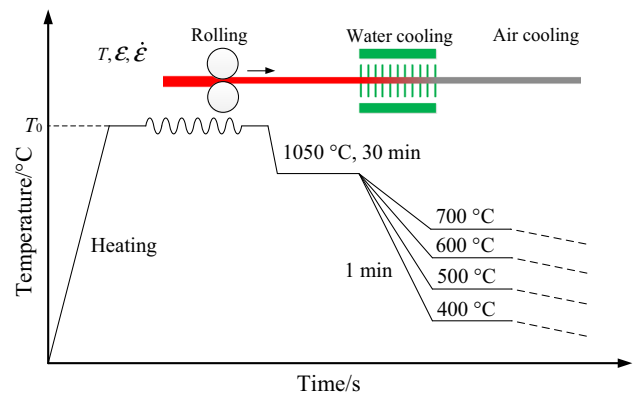


Fig. 3 Schematic diagram of hot rolling and heat treatment process

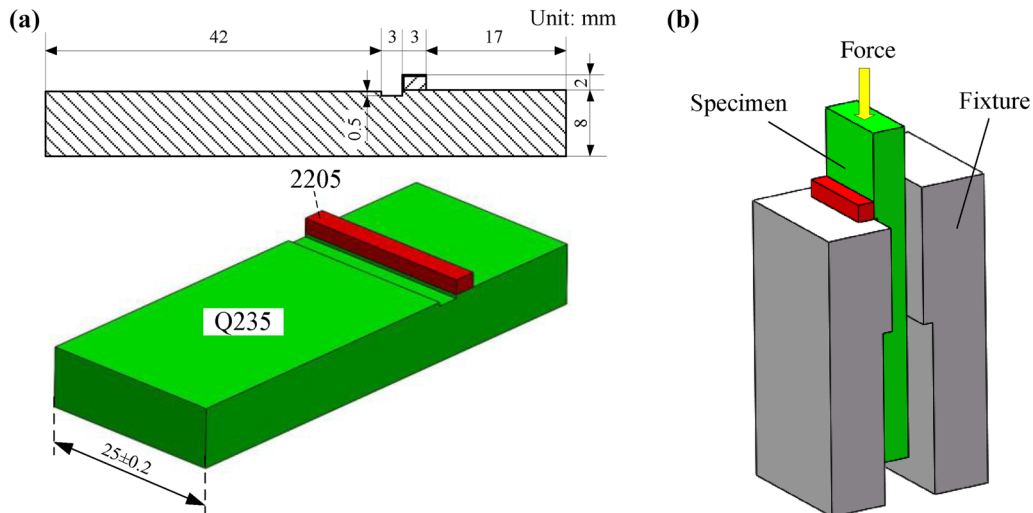


Fig. 4 Shear strength test for 2205/Q235 bonding interface. **a** Specimen; **b** shear strength test

on a material universal testing machine [23]. Optical microscopy, scanning electron microscopy and energy-dispersive spectrum analysis were used to evaluate the microstructure of 2205/Q235 DSS clad plate prepared by vacuum hot rolling.

3 Results and discussion

3.1 Stress–strain curves and processing map of 2205

As shown in Fig. 5, the stress–strain curves of 2205 DSS were obtained. The processing map was established by

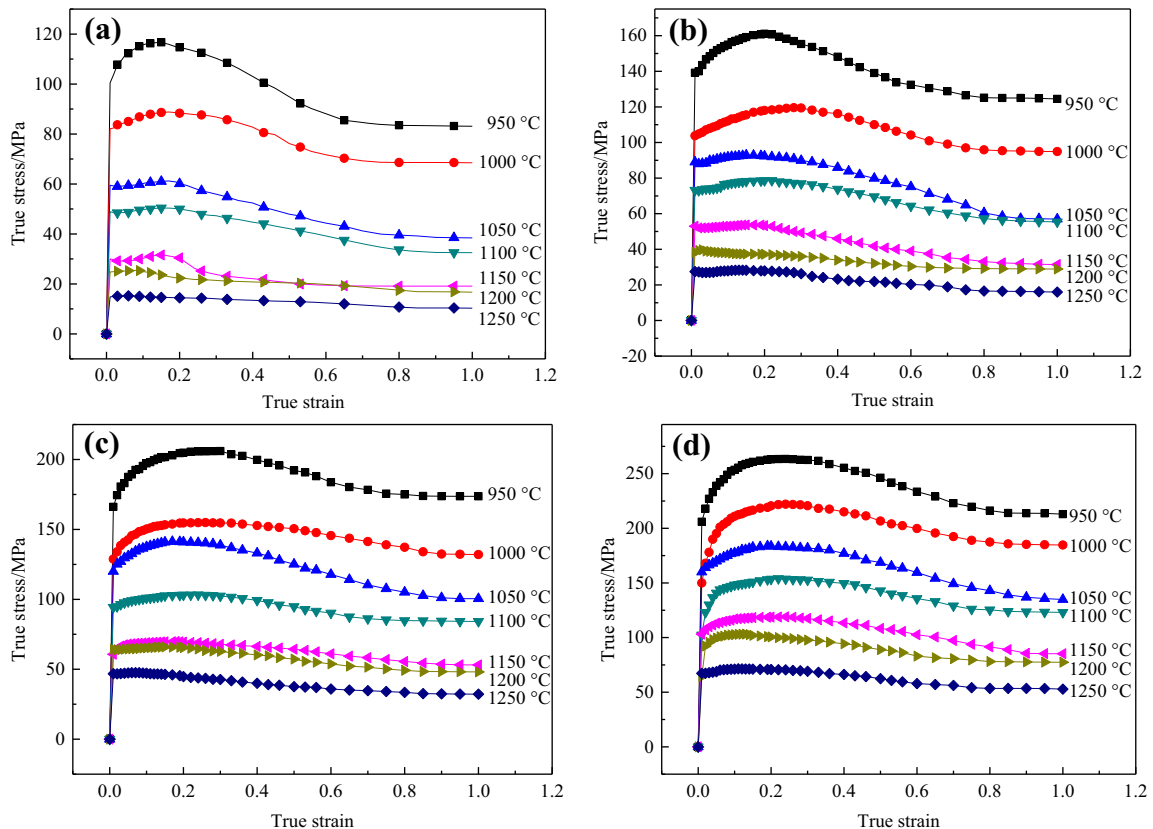


Fig. 5 Flow stress of 2205 DSS. **a** $\dot{\epsilon} = 0.01 \text{ s}^{-1}$; **b** $\dot{\epsilon} = 0.1 \text{ s}^{-1}$; **c** $\dot{\epsilon} = 1 \text{ s}^{-1}$; **d** $\dot{\epsilon} = 10 \text{ s}^{-1}$

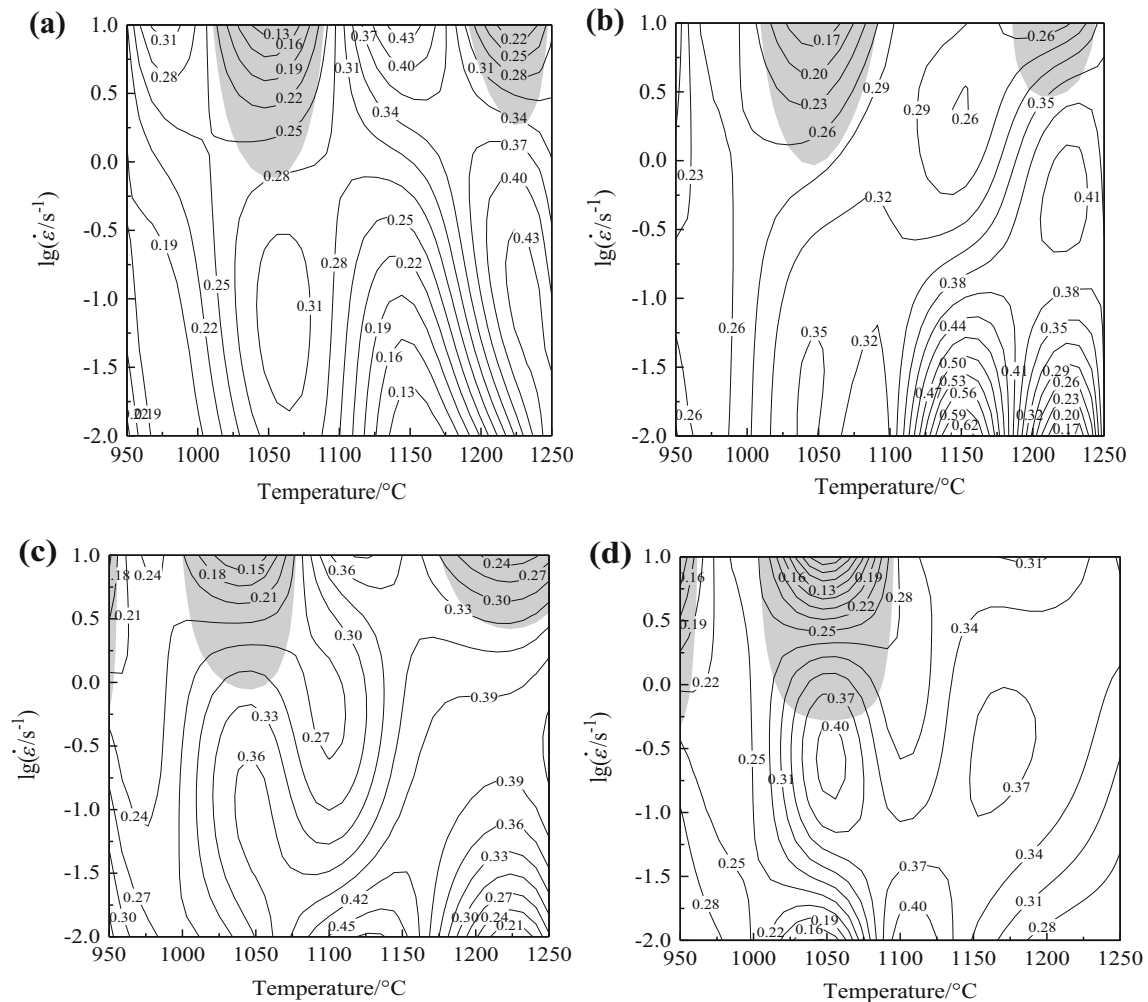


Fig. 6 Processing map of 2205 DSS. **a** $\varepsilon = 0.1$; **b** $\varepsilon = 0.4$; **c** $\varepsilon = 0.7$; **d** $\varepsilon = 1.0$

using the tested data according to dynamic materials modeling (Fig. 6) [24]. From the processing map, the hot working process window can be attained. The instability zones of flow behavior can also be recognized by the maps. It can also be found that the efficiency of power dissipation η increases first and then decreases with increasing deformation temperature and decreasing strain rate, and the efficiency peak at various strains appears in different locations.

3.2 Temperature field of clad plate in rolling process

The numerical simulation results show that the temperature of 2205 clad material in the rolling process changed from 1200 to 1210 °C when the initial rolling temperature was 1200 °C and the rolling reduction was 10, 20, 30 and 40%, respectively. Figure 7 shows the nephogram of temperature field when the rolling reduction was 40%. It was proved that the four-layer symmetrical packing method could

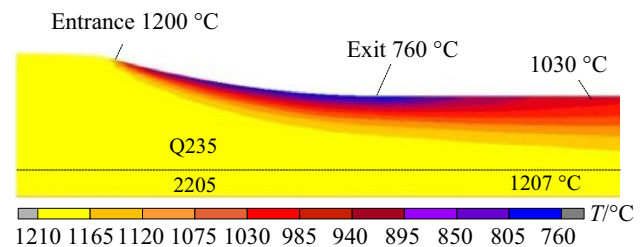


Fig. 7 Temperature distribution of clad sheet with rolling reduction of 40%

guarantee that the temperature of 2205 DSS was almost constant in the rolling process, which effectively avoided the appearance of micro-cracks.

3.3 Deformation behavior under different rolling speeds and reductions

In the practical production, the deformation behavior depends on the rolling speed and reduction. Figure 8 shows

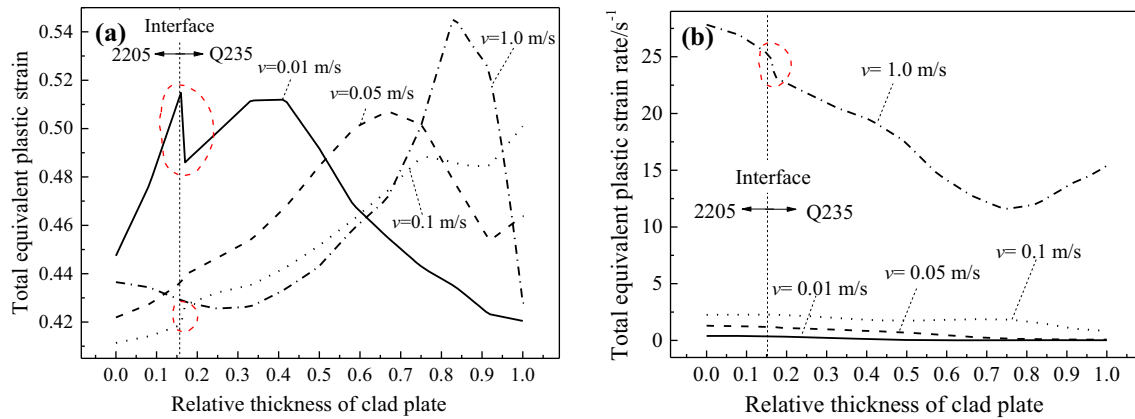


Fig. 8 Equivalent plastic strain (a) and total equivalent plastic strain rate (b) of clad plates under different rolling speeds

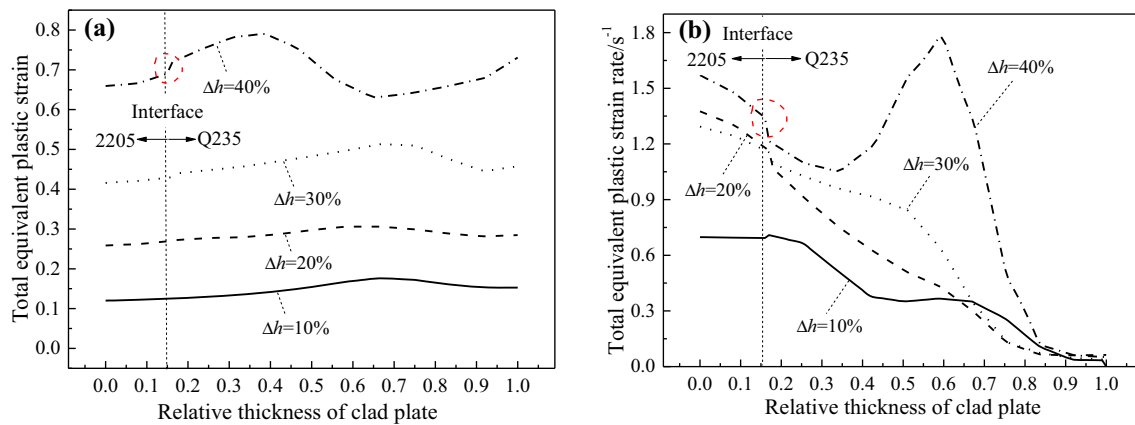


Fig. 9 Equivalent plastic strain (a) and total equivalent plastic strain rate (b) of clad plates under different reductions

the simulation result of 2205/Q235 clad plate when the rolling reduction was 30% and the rolling speed increased from 0.01 to 1.00 m/s. As shown in Fig. 8a, the equivalent plastic strain on the interface changed suddenly when rolling speed was 0.01 and 0.10 m/s, leading to non-compatible deformation. To achieve the compatibility of interlamellar deformations of 2205/Q235 clad plate, the rolling speed should be chosen as 0.05 and 1.00 m/s. However, the strain rate of 2205 DSS increased with the increase in rolling speed, as shown in Fig. 8b. As the ferrite phase is soft and the austenite phase is hard at the same high temperature, the micro-cracks between the two phases easily form due to the high strain rate. Thus, the strain rate should be as small as possible. Therefore, the optimum rolling speed was chosen as 0.05 m/s.

Figure 9 shows the simulation results of 2205/Q235 clad plate when the rolling reduction increased from 10 to 40% and the rolling speed was 0.05 m/s. The equivalent plastic strain and strain rate on the clad interface increased when the rolling reduction increased from 10 to 40%. With increasing power dissipation efficiency, the dynamic softening of austenite was more obvious, and the difference of

deformation characteristics between austenite and ferrite was getting smaller. Thus, the micro-cracks could be avoided effectively. As it can be seen in the processing map, the optimum temperature was 1210–1230 °C ($\eta = 0.41$) when rolling speed was 0.05 m/s ($\dot{\epsilon} = 1.0$ – 1.2 s^{-1}) and rolling reduction was 30–40% ($\epsilon = 0.43$ – 0.52).

3.4 Critical thickness for different cooling conditions

The cooling rate at the plate center is determined by the cooling condition and the thickness of the clad plate. High cooling rate can be achieved with greater cooling intensity and thin plate. The present works indicated that the 2205 DSS should be cooled from 1050 to 500 °C within 1 min to form uniform dual-phase structure of ferrite and austenite. Figure 10 shows the critical thickness of the clad plate for different conditions. It can be seen that the critical thickness was 23, 31 and 42 mm when λ_1 was 1.0, 1.5 and 2.8 $kW/(m^2 K)$, respectively [20]. It provides foundation to design the water flow rate used in fast cooling process after hot rolling in the following pilot experiment.

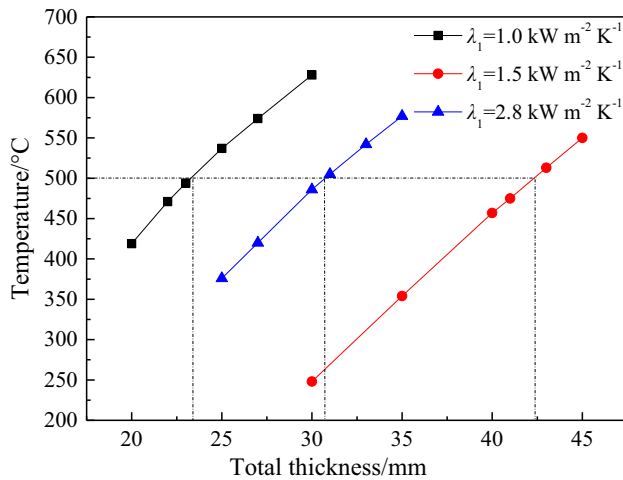


Fig. 10 Critical thickness of clad plate for different cooling conditions

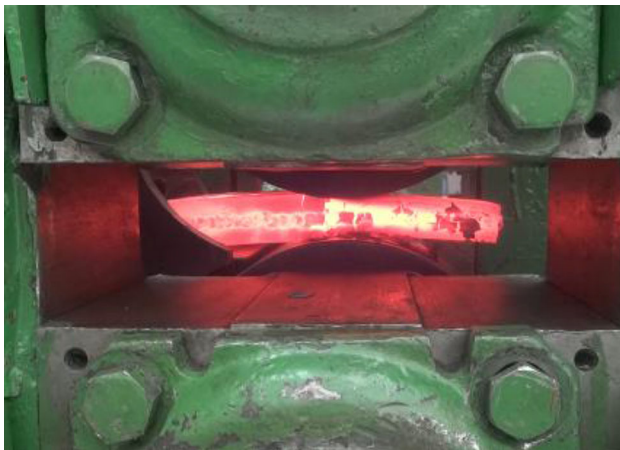


Fig. 11 Rolling pilot experiment

3.5 Performance and microstructure of 2205/Q235 clad plate prepared by pilot experiments

As shown in Fig. 11, the pilot experiments were carried out with above optimized parameters and the 2205/Q235 clad plates have been successfully prepared. The shear strength tests were conducted, and the results under different rolling reductions are shown in Fig. 12. The shear strength of bonding interface increased from 120 to 530 MPa when the rolling reduction increased from 10 to 40%. Thereinto, when the reductions were 30 and 40%, the shear strength exceeded the requirements of Chinese national standard (210 MPa).

As shown in Fig. 13, the fracture morphology of specimens with 40% rolling reduction was analyzed by scanning electron microscopy. The fracture was considered to be ductile as there were obvious dimple tissues at the

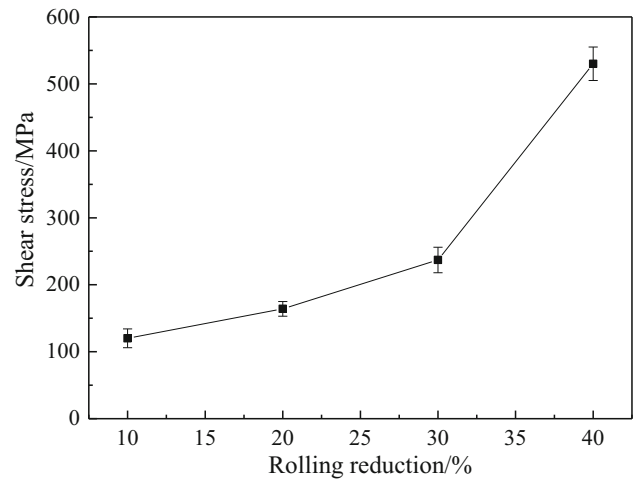


Fig. 12 Shear strength of bonding interface

fracture. Under shear loading conditions, a mass of dislocations appeared in the clad interface, and different sizes of micro-holes were gradually formed with increasing load. When the micro-holes gathered and formed the dimple tissues of different sizes, the fracture of clad interface appeared. Thus, it can be concluded that the composite effect was excellent. The white particles on the shear cross section were oxides by energy-dispersive spectrum analysis, which were mainly composed of Fe, O, Mn, S, Al and Mg elements. As the oxides on the fracture surface were quite small and scarce, it can be considered that the oxide particles had little significant effect on the plastic toughness of clad interface.

Figure 14 shows the metallograph of four cooling paths for clad plate with rolling reduction of 40%. When the ending temperature of 2205 DSS in the heat treatment process was 500 °C, there was only two-phase structure of ferrite and austenite in 2205 DSS, with ferrite and austenite of 55.98% and 44.02%, respectively. No micro-cracks were found in the boundaries between ferrite and austenite and in the ferrite. Other phases appeared in the phase boundary in addition to the ferrite and austenite phases in other three cooling paths. Therefore, the optimum cooling path was quickly cooling to 500 °C within 1 min.

Figure 15 shows the results of the microstructure and line scan of the clad interface. It indicates that the elements on both sides of the interface, especially Fe and Cr, were diffused. The thickness of the clad layer was about 42 μm at four cooling paths, which indicates that the thickness of diffusion layer was not affected by cooling mode. Therefore, the thickness of diffusion layer could be mainly regulated through adjusting the holding time.

Figure 16 shows the results of backscattered scanning electron microscopy and spot scan of clad interface with rolling reduction of 40% and quickly cooling to 500 °C

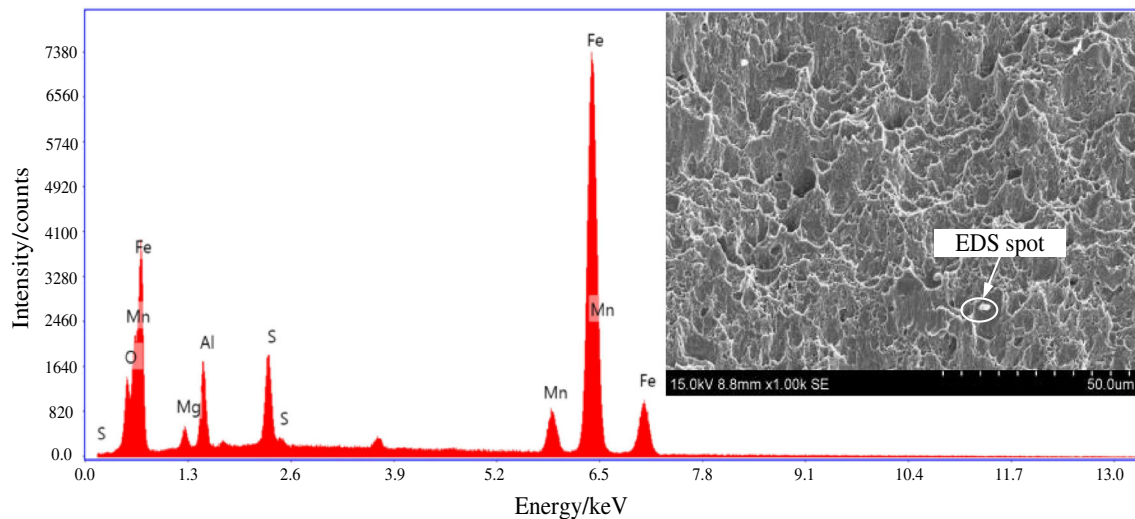


Fig. 13 Shear fracture morphologies and oxide analysis

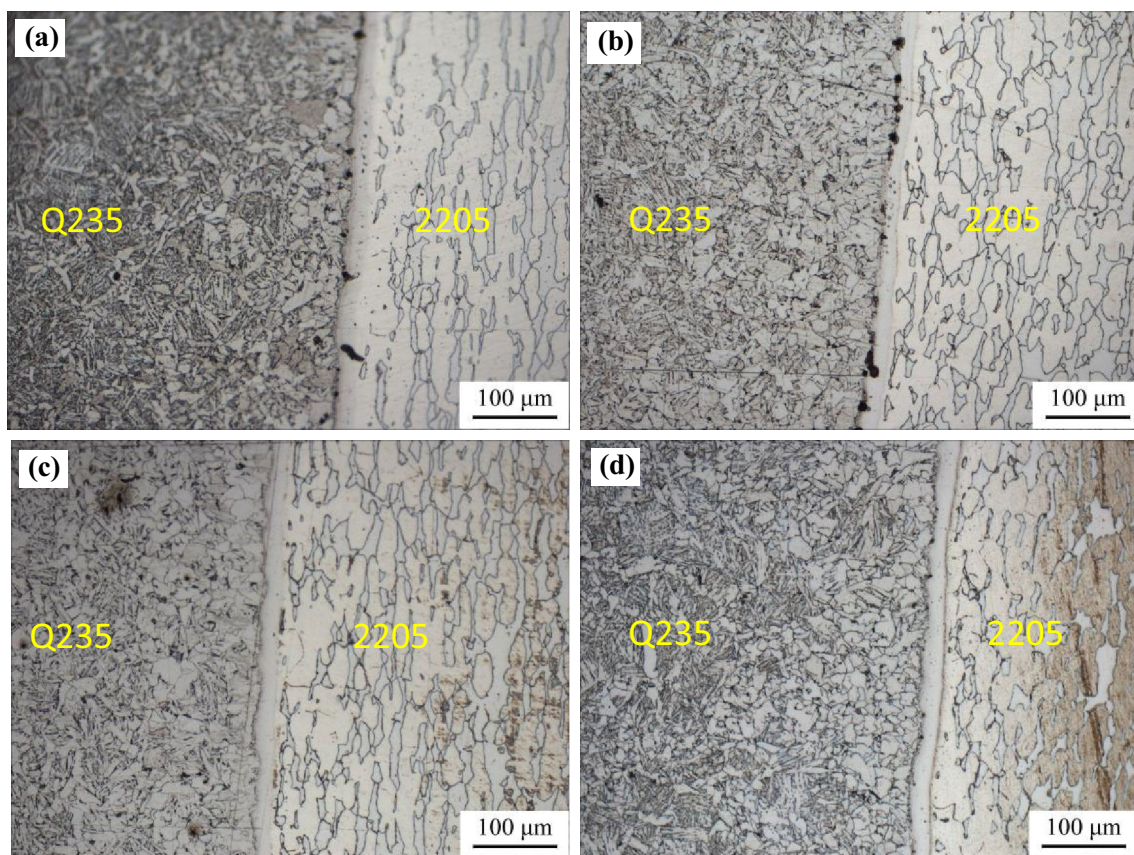


Fig. 14 Bonding interface morphology after heat treatment at different ending temperatures. **a** $T_e = 400\text{ }^\circ\text{C}$; **b** $T_e = 500\text{ }^\circ\text{C}$; **c** $T_e = 600\text{ }^\circ\text{C}$; **d** $T_e = 700\text{ }^\circ\text{C}$

within 1 min. As shown in Fig. 16, the scanning spots are 2205 matrix (spot 1), Q235 matrix (spot 2), the clad interface near 2205 matrix (spot 3) and the clad interface near Q235 matrix (spot 4), respectively. The scanning spots

5–7 are the compounds in the bonding interface. Table 3 shows the element contents of each scanning spot.

Through the comparison between scanning spots 1–4, it can be known that the N, Cr, Mo, Ni, Si and Mn elements

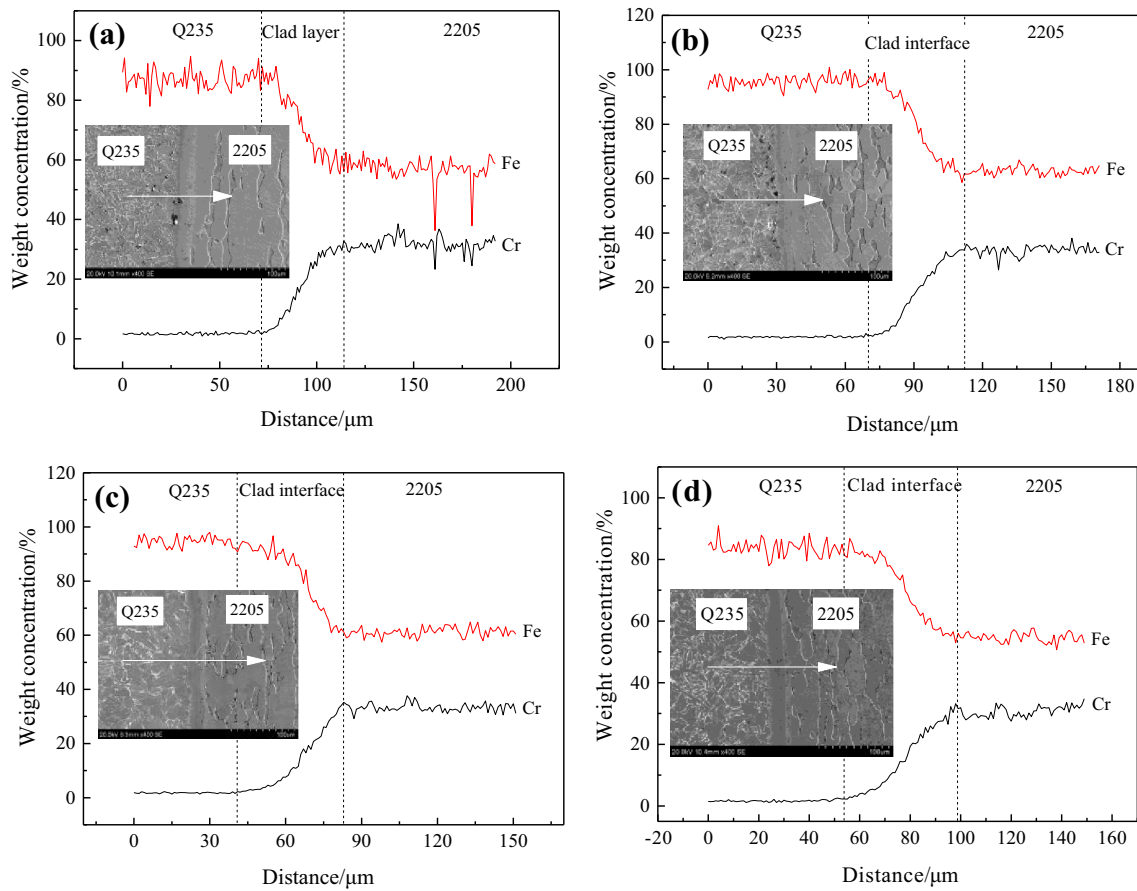


Fig. 15 Microstructure and line scan of clad sheet interface at different heat treatment ending temperatures. **a** $T_e = 400\text{ }^\circ\text{C}$; **b** $T_e = 500\text{ }^\circ\text{C}$; **c** $T_e = 600\text{ }^\circ\text{C}$; **d** $T_e = 700\text{ }^\circ\text{C}$

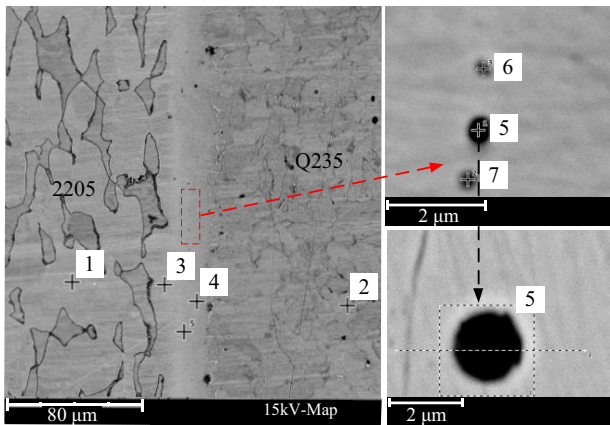


Fig. 16 Measurement points of spot scan

contents of clad interface were gradually increased and the C element content was gradually decreased from Q235 to 2205 steel. Due to the diffusion of elements, a white uniform-striped zone was formed in the clad interface (as seen in Fig. 16). The comparison among scanning spots 1, 3 and 4 indicated that the element composition of clad interface

Table 3 Main element contents of scanning spots (mass%)

Spot	C	N	Cr	Ni	Si	Mo	Mn	Fe
1	0.04	0.12	19.2	4.36	0.51	2.61	1.10	72.06
2	0.16	0.003	0.3	0.27	0.26	0.04	0.69	98.28
3	0.05	0.09	16.8	4.2	0.45	2.54	0.92	69.81
4	0.08	0.05	11.2	1.23	0.33	1.21	0.80	82.35
Spot	Fe	O	C	Cr	Si	Mo	Mn	
5	41.4	21.3	7.83	6.02	0.85	0.87	1.74	
6	56.1	12.3	14.2	7.56	1.05	1.47	1.77	
7	53.9	11.5	4.82	7.58	1.01	1.04	1.76	

was close to the austenite structure of 2205 DSS. In other words, the clad interface can be seen as a new-type microstructure of austenitic stainless steel. In the meanwhile, the microstructure of clad interface was slightly varied with the interface location.

Some micro-compounds were also observed in the clad interface. As the 2205 DSS was quite sensitive to the C element, it is speculated that the compounds were $M_{23}C_6$

carbide due to the C element diffusion from Q235 steel. According to the results of spot scan, the contents of oxygen were 21.3, 12.3 and 11.5% in scanning spots 5–7, respectively; it was ensured that the compounds were oxide from the residual oxygen. As the oxide may be a fracture origin, the residual oxide should be reduced and cleaned up with improving the vacuum degree.

4 Conclusions

1. Referring to the pack rolling method, the Q235/2205/2205/Q235 four-layer symmetrical assembling method and vacuum hot rolling were successfully applied in fabrication of 2205/Q235 clad plate by establishing a relatively stable thermo-mechanical environment for 2205 DSS.
2. According to the hot working behavior from processing map of 2205 DSS, numerical simulation and pilot experiments were carried out to achieve the optimum rolling and heat treatment parameters.
3. In order to achieve satisfactory bonding strength, mechanical properties, as well as corrosion resistance performance, the optimum rolling temperature was 1210–1230 °C when rolling speed was 0.05 m/s ($\dot{\epsilon} = 1.0\text{--}1.2\text{ s}^{-1}$) and rolling reduction was 30–40% ($\epsilon = 0.43\text{--}0.52$). And the cooling rate of 2205 steel should be greater than 10 °C/s between 1050 and 500 °C after rolling.

Acknowledgements The authors would like to acknowledge the National Natural Science Foundation of China (Grant Nos. 51474189 and 51674222), the Natural Science Foundation of Hebei Province Distinguished Young Fund Project (Grant No. E2018203446) and the Educational Commission of Hebei Province (QN2015214).

References

- [1] Z.G. Song, H. Feng, S.M. Hu, *J. Iron Steel Res. Int.* 24 (2017) 121–130.

- [2] J.L. Lv, T.X. Liang, C. Wang, L.M. Dong, *Mater. Sci. Eng. C* 62 (2016) 558–563.
- [3] Z.Y. Bi, J.X. Zhang, F. Zhang, S.L. Jin, *Corrosion & Protection* 31 (2010) 349–352.
- [4] H. Farnoush, A. Momeni, K. Dehghani, J.A. Mohandesi, H. Keshmiri, *Mater. Des.* 31 (2010) 220–226.
- [5] T. Kannan, N. Murugan, *J. Mater. Process. Technol.* 176 (2006) 230–239.
- [6] B. Senthilkumar, T. Kannan, *Procedia Eng.* 64 (2013) 1030–1039.
- [7] X.J. Di, Z.T. Zhong, C.Y. Deng, D.P. Wang, X.J. Guo, *Mater. Des.* 95 (2016) 231–236.
- [8] Z.A. Luo, G.L. Wang, G.M. Xie, L.P. Wang, K. Zhao, *Acta Metall. Sin. (Engl. Lett.)* 26 (2013) 754–760.
- [9] G. Lin, Z.X. Zhang, H.W. Song, J. Tong, C.D. Zhou, *J. Iron Steel Res. Int.* 15 (2008) No. 6, 83–86.
- [10] J.M. Cabrera, A. Mateo, L. Llanes, J.M. Prado, M. Anglada, *J. Mater. Process. Technol.* 143–144 (2003) 321–325.
- [11] M. Balbi, M. Avalos, A. El Bartali, I. Alvarez-Armas, *Int. J. Fatigue* 31 (2009) 2006–2013.
- [12] L.Y. Yu, H. Luo, X.Y. Li, *Heat Treatment of Metals* 35 (2010) No. 3, 50–53.
- [13] R. Kaçar, M. Acarer, *Mater. Sci. Eng. A* 363 (2003) 290–296.
- [14] Q. Sun, J. Wang, H.B. Li, Y. Li, Y.D. Hu, J.G. Bai, P.D. Han, *J. Iron Steel Res. Int.* 23 (2016) 1071–1079.
- [15] H. Zhou, F. Kong, X. Wang, Y. Chen, *J. Alloy. Compd.* 695 (2017) 3495–3502.
- [16] J.L. Qu, J.H. Du, Q. Deng, J.Y. Zhuang, X.D. Lu, *Materials Science & Technology* 16 (2008) No. 1, 121–124.
- [17] H. Zhang, J.H. Peng, Z. Zhang, Z.H. Zhong, Y.C. Zheng, Y.C. Wu, *Heat Treatment of Metals* 42 (2017) No. 3, 108–112.
- [18] H. Utsunomiya, M.P.F. Sutcliffe, H.R. Shercliff, P. Bate, D.B. Miller, *Int. J. Mech. Sci.* 46 (2004) 1349–1364.
- [19] T.L. Fu, Z.D. Wang, Y. Li, J.D. Li, G.D. Wang, *Journal of Harbin Institute of Technology (New Series)* 21 (2014) No. 2, 57–62.
- [20] H.M. Wang, Q.W. Cai, W. Yu, L. Su, *J. Univ. Sci. Technol. Beijing* 34 (2012) 1421–1425.
- [21] B.X. Liu, F.X. Yin, X.L. Dai, J.N. He, W. Fang, C.X. Chen, Y.C. Dong, *Mater. Sci. Eng. A* 679 (2017) 172–182.
- [22] J.J. Zhang, R.S. Liu, H.Y. Zhao, S. Yue, *Chinese Materials Science Technology & Equipment* 4 (2007) No. 6, 84–86.
- [23] H.G. Huang, Z.W. Lv, M. Yan, F.S. Du, *Journal of Basic Science and Engineering* 23 (2015) 1266–1274.
- [24] S. Masuda, I. Nakauchi, A. Tagane, M. Yamawaki, *Trans. Iron Steel Inst. Jpn.* 28 (1988) 470–477.